The Journal of Physiology

https://jp.msubmit.net

JP-RP-2023-285475R1

Title: PRE-INTERVENTION MYOCARDIAL STRESS IS A GOOD PREDICTOR OF AORTIC VALVOLUPLASTY OUTCOME FOR FETAL CRITICAL AORTIC STENOSIS AND EVOLVING HLHS

Authors: Laura Green
Wei Xuan Chan
Indumita Prakash
Andreas Tulzer
Tulzer Gerald
Choon Hwai Yap

Author Conflict: No competing interests declared

Author Contribution: Laura Green: Conception or design of the work; Acquisition, analysis or interpretation of data for the work; Drafting the work or revising it critically for important intellectual content; Final approval of the version to be published; Agreement to be accountable for all aspects of the work Wei Xuan Chan: Acquisition, analysis or interpretation of data for the work; Drafting the work or revising it critically for important intellectual content; Final approval of the version to be published; Agreement to be accountable for all aspects of the work Indumita Prakash: Acquisition, analysis or interpretation of data for the work; Drafting the work or revising it critically for important intellectual

content; Final approval of the version to be published; Agreement to be accountable for all aspects of the work Andreas Tulzer: Acquisition, analysis or interpretation of data for the work; Drafting the work or revising it critically for important intellectual content; Final approval of the version to be published; Agreement to be accountable for all aspects of the work Tulzer Gerald: Acquisition, analysis or interpretation of data for the work; Drafting the work or revising it critically for important intellectual content; Final approval of the version to be published; Agreement to be accountable for all aspects of the work Choon Hwai Yap: Conception or design of the work; Acquisition, analysis or interpretation of data for the work; Drafting the work or revising it critically for important intellectual content; Final approval of the version to be published; Agreement to be accountable for all aspects of the work

Running Title: Myocardial stress predicts fetal aortic valvuloplasty outcomes well

Dual Publication: No

Funding: Imperial College London (ICL): Laura Green, PhD Scholarship; BHF Centre of Research Excellence, Imperial College: Wei Xuan Chan, RE/18/4/34215

PRE-INTERVENTION MYOCARDIAL STRESS IS A GOOD PREDICTOR OF AORTIC VALVOLUPLASTY OUTCOME FOR FETAL CRITICAL AORTIC STENOSIS AND EVOLVING HLHS

Laura Green[1], Wei Xuan Chan[1,2], Indumita Prakash[1], Andreas Tulzer[3,4], Gerald Tulzer[3,4], Choon Hwai Yap[1]

[1] *Department of Bioengineering, Imperial College London, London, United Kingdom*

[2] *BHF Centre of Research Excellence, Imperial College London, London, United Kingdom*

[3] *Department of Pediatric Cardiology, Children's Heat Center Linz, Kepler University Hospital, Linz, Austria*

[4] *Medical Faculty, Johannes Kepler University Linz, Altenberger Strasse 69, 4040 Linz, Austria*

Correspondence: *Choon Hwai Yap,* c.yap@imperial.ac.uk

First Author Profile: Laura Green is currently pursuing a PhD at Imperial College London within the Cardiovascular Biomechanics and Ultrasound Laboratory, under the guidance of Dr Choon Hwai Yap. Her research is dedicated to advancing understanding of fetal left ventricular biomechanics, with a particular focus on investigating the impact critical aortic stenosis with evolving hypoplastic left heart syndrome has on fetal cardiac functionality, both before and after fetal aortic valvuloplasty intervention.

KEY POINTS

- Predicting the morphological birth outcomes (univentricular versus biventricular) of fetal aortic valvuloplasty for fetal aortic stenosis with evolving HLHS is important for accurate patient selection, parental counseling and management decisions.
- Computational simulations show that a biomechanics parameter, pre-intervention peak systolic myofiber stress, is uniquely robust in distinguishing between such outcomes, outperforming all echo parameters.
- An empirical equation was developed to quickly compute peak systolic myofiber stress from routine echo measurements and was the best predictor of outcomes among a wide range of parameters tested.

ABSTRACT

Fetal critical aortic stenosis with evolving hypoplastic left heart syndrome (CAS-eHLHS) causes biomechanical and functional aberrations, leading to a high risk of progression to HLHS at birth. Fetal aortic valvuloplasty (FAV) can resolve outflow obstruction and may reduce progression risk. However, it is currently difficult to accurately predict which patients will respond to the intervention and become functionally biventricular (BV) at birth, as opposed to becoming functionally univentricular (UV). This prediction is important for patient selection, parental counselling, and surgical planning. Therefore, we investigated whether biomechanics parameters from pre-FAV image-based computations could robustly distinguish between CAS-eHLHS cases with BV or UV outcomes in a retrospective cohort. To do so we performed image-based finite element biomechanics modelling of 9 CAS-eHLHS cases undergoing intervention and 6 healthy fetal control hearts, and found that a biomechanical parameter, peak systolic

myofiber stress, showed a uniquely large difference between BV and UV cases, which had a larger effect magnitude than echocardiography parameters. A simplified equation was derived for quick and easy estimation of myofiber stress from echo measurements via principal component analysis. When tested on a retrospective cohort of 37 CAS-eHLHS cases, the parameter outperformed other parameters in predicting UV versus BV outcomes, and thus have a high potential of improving outcome predictions if incorporated into patient selection procedures. Physiologically, high myocardial stresses likely indicate a healthier myocardium that can withstand high stresses and resist pathological remodeling, which can explain why it is a good predictor of BV outcomes.

Keywords: cardiac biomechanics, evolving hypoplastic left heart syndrome, fetal aortic valvuloplasty, fetal critical aortic stenosis, finite element modelling

---

INTRODUCTION

In selected fetal hearts with critical aortic stenosis (CAS), natural history studies shown there to be a 73% likelihood of progression to hypoplastic left heart syndrome (HLHS) by the time of birth, and for this reason, was named CAS with evolving HLHS (CAS-eHLHS) (Mäkikallio *et al.*, 2006; Gardiner *et al.*, 2016). Progression to HLHS was especially likely for cases with retrograde transverse aortic arch flow, left-to-right flow across the foramen ovale, and monophasic mitral inflow. The aortic obstruction in these cases leads to high left ventricular (LV) pressure, globular LV shapes, hypertrophy of LV walls, diminished LV contractile deformation, high aortic valve (AV) velocity, endocardial fibroelastosis and mitral valve regurgitation (MVr), which also causes high left atrial (LA) pressure and LA distension (Tulzer & Arzt, 2013). These abnormalities are likely detrimental to the growth of the LV and cause of subsequent hypoplastic development which leads to a univentricular (UV) outcome.

In such cases, fetal aortic valvuloplasty (FAV) was found to be promising, by reducing the risk of progression to HLHS (Mäkikallio *et al.*, 2006; Gardiner *et al.*, 2016; Friedman *et al.*, 2018; Tulzer *et al.*, 2022*a*). FAV is a catheter-based intervention which widens the aortic obstruction to improve several of the above abnormal features, which will likely restore LV growth to prevent a UV outcome. However, high volume institutions have shown FAV to carry with it a 4-8% chance of fetal demise (Pickard *et al.*, 2020; Tulzer *et al.*, 2022*b*). A recent cost-benefit analysis showed that FAV confers a modest medium-term (age 6) survival benefit from 72% to 82% (Pickard *et al.*, 2020).

Current patient selection criteria for FAV includes the presence of LV systolic and diastolic dysfunction, retrograde bidirectional transverse aortic arch flow, a LV long axis Z-score<-2, dilated LV, left to right shunting through the foramen ovale and MVr or aortic stenosis gradient >20 mmHg (Tulzer & Arzt, 2013; Friedman *et al.*, 2018). However, a substantial proportion of fetuses selected for FAV did not avoid progression to UV outcome, even with a successful intervention, suggesting a current inability to accurately predict outcomes, and that current selection criteria for the intervention can be refined to more accurately identify patients that will benefit from the intervention. More accurate prediction can better inform decisions on whether to proceed with the intervention, given that there are significant procedural risks to fetuses. It may also lead to the identification of cases that are likely to respond to the intervention, but that are outside of the current selection criteria. For this reason, there has been continued investigation into biomarkers that are indicative of outcomes (Friedman *et al.*, 2018; Prosnitz *et al.*, 2018; Beattie *et al.*, 2020; Tulzer *et al.*, 2022*a*).

Biomechanics evaluation of the CAS-eHLHS fetal heart, or the investigation of its force dynamics in relation to its motion and deformation, is important. The CAS-eHLHS heart has drastically different

biomechanical characteristics from the healthy heart, the FAV intervention is essentially a mechanical intervention in nature, and the heart is likely to be mechanosensitive in its growth, where abnormal biomechanics may play a significant role in the progression to malformation. Cardiac Finite Element (FE) computational modelling is a good approach for investigating myocardial biomechanics and has been very useful in improving our understanding of multitude of heart diseases in the past (Dewan *et al.*, 2017; Ong *et al.*, 2020; Wisneski *et al.*, 2020; Shavik *et al.*, 2021). For example, we have previously used such a model to elucidate the effects of how various CAS-eHLHS characteristics impact cardiac function and biomechanics (Ong *et al.*, 2020). Further, a previous FE model coupled with a myocardial growth mathematical model showed that reduced strain stimuli can potentially explain the gestational development of some HLHS cases (Dewan *et al.*, 2017). FE modelling performs an assessment of the physics of the heart's function and can provide biomechanics parameters that are difficult to directly obtain from clinical measurements, such as myocardial stresses and the extent of active tension generation, which may be useful for predicting outcomes.

Here, we performed image-based, patient-specific FE modelling of CAS-eHLHS and healthy hearts to elucidate the biomechanical characteristics of the disease. We hypothesize that the biomechanics parameter of myocardial stress, obtained at a pre-interventional stage for CAS-eHLHS cases undergoing FAV, may show a better association with UV or BV outcomes compared with clinical measurements, and thus has the potential of being a better predictive biomarker.

MATERIALS AND METHODS

Ethical Approval

9 CAS-eHLHS datasets and 1 healthy dataset were obtained with informed consent in writing from the Kepler University Hospital, Austria, under Institutional Review Board protocol 1009/2017. The remaining healthy datasets were obtained also with written informed consent from National University Hospital Singapore under Domain Specific Review Board protocol 2014/00056. The studies conform to latest revision of the Declaration of Helsinki, except for registration in a database.

Image Acquisition

4D echocardiography images of 9 fetal hearts with CAS-eHLHS undergoing FAV and 6 healthy hearts were acquired using the GE Voluson E10 (GE Healthcare, Chicago, IL, USA) ultrasound machine. Images were taken in the spatio-temporal image correlation mode, using the standard settings of sweeps of 10-15s and capture rate of 70-90 frames per second. Of the 9 CAS-eHLHS cases, 5 went on to achieve a functionally BV heart at birth, 4 went on to be functionally UV at birth.

2D echocardiography and Doppler measurements for a further 28 CAS-eHLHS fetuses undergoing intervention, acquired with the Vivid E95, were also obtained from Linz Hospital, Austria and were further used together with the first 9 CAS-eHLHS cases for analysis on predictive capabilities of various parameters. Since the original 9 CAS-eHLHS cases were used to develop the empirical equation without referencing their BV versus UV outcomes, they were still eligible for use when testing for how well parameters can predict outcomes.

Patient Characteristics

Healthy control cases were from ages of 21+2 wks+days to 32+0 wks+days gestation. At the time of study all CAS-eHLHS patients that had complete datasets with clear 4D volume images were used. The CAS-eHLHS patients were selected for FAV intervention at Linz Hospital, Austria, if they exhibited the following characteristics: dilated and poorly contracting LV, left to right shunting at atrial level, retrograde aortic arch flow, LV length Z-score >0 or RV/LV ratio >1.1 and no signs of AV atresia. The CAS-

eHLHS patients ranged from 22+4 wks+days to 32+0 wks+days gestation. Age matched healthy control cases for CAS-eHLHS patients were not available, so a range of healthy cases were selected that encapsulated the age range of CAS-eHLHS patients.

Characteristics of patients included in the study are given in Table 1, including age, disease features and postnatal outcomes and postnatal procedures. Throughout the study, the disease cases with a BV birth outcome were denoted by 'BV' in front of the ID number, while those with a UV outcome were denoted by 'UV' in front of the ID number. Healthy cases were denoted by a 'H', in front of the ID number. A BV circulation postnatal outcome was defined when the LV was the only source of systemic circulation and where there was an absence of pulmonary hypertension at 1 year of age. Diseased cases outside of this definition were designated to be a UV outcome. Analyses were performed to determine which pre-interventional features were correlated to outcomes and have a potential to be used for outcome predictions. Postnatal procedures for cases with BV outcomes included AV dilation or the Ross-Kono procedure, while that for cases with UV outcomes included the Norwood procedure or a Ross-Kono with subsequent BV-UV conversion.

Image Processing of Fetal Echocardiography

From the fetal echo images, morphometric measurements of the heart chambers, including LV and RV longitudinal length, posterior wall thickness (PWT), LV inner diameter at diastole (LVID), and relative wall thickness (RWT) were performed in accordance with previous approaches (Tulzer *et al.*, 2022*a*), by 2 independent observers, repeated twice per person, and averaged. RWT is calculated as,

$$RWT = \frac{2 \times PWT}{LVID}. \qquad \text{Equation 1}$$

and aspect ratio was calculated as,

$$Aspect\ ratio = \frac{LVID}{LV\ Length}. \qquad \text{Equation 2}$$

Patient-specific reconstruction of 3D computational models of fetal hearts were obtained using methods previously described (Ong *et al.*, 2020). In brief, stacked 2D images were extracted from the 4D scans, at 0.5 mm intervals, at a specific time point. A Lazy Snap algorithm (Li *et al.*, 2004) was then used to trace the endocardial and epicardial boundaries and the traced slices were reconstructed using a Vascular Modeling Toolkit (VMTK). Any irregularities in the reconstructed geometry were smoothed in Geomagic (Geomagic Inc., Morrisville, USA). Figure 1 depicts all patient specific geometries modelled in this study.

A validated cardiac motion estimation algorithm (Wiputra *et al.*, 2020) was then used to extract cardiac motions, which was used to animate the heart chambers over the cardiac cycle and obtain reconstructions and chamber volumes for all other time points (Figure 2). Briefly the cardiac motion was modelled as a cyclic and spatially consistent b-spline of Fourier whole-field motion model and was curve-fitted to the displacement fields from pair-wise image registration of images from all consecutive time frames (Wiputra et al., 2020). Using the estimated cardiac motion, the reconstructed LV geometry at end diastolic volume (EDV) was animated over the cardiac cycle. For CAS-eHLHS diseased LVs, motion was diminished, and therefore this process was sufficient when extracting accurate motions from images. For healthy LVs, greater cardiac motions and deformations occurred, and reconstruction at end-systole was needed to enhance motion estimation, by including the registration results of the end-diastole to end-systole time points to the curve fitting, as previously described (Wiputra et al., 2020).

LV myocardial engineering strains (Equation 3) were computed from the images in both the longitudinal and circumferential directions along a mid-wall line, identified by averaging the epicardial and endocardial boundaries, from the 4-chamber or transverse echo view, using previously documented

techniques (Ren *et al.*, 2023). The mid-wall line was discretized into 100 elements, its motion was tracked, and changes in lengths of elements from end diastole to end systole were computed and spatially averaged,

$$Engineering\ Strain = \frac{Length_{systole} - Length_{diastole}}{Length_{diastole}}. \quad \text{Equation 3}$$

The engineering strains measured will be reported as circumferential and longitudinal strains throughout the remainder of the study.

Computational Modelling Methods

Image-based, patient-specific FE Modelling of fetal LV myocardial biomechanics was performed in accordance with our previous methodologies (Ong *et al.*, 2020; Green *et al.*, 2022). The FE model was connected to a lumped parameter model to enable ventricular-vascular coupling.

LV myocardium models reconstructed from echo images were used for FE modelling and were meshed into a minimum of 2,500 quadratic tetrahedral elements (Figure 3A), which was sufficient for mesh convergence as shown in our previous study (Ong *et al.*, 2020). A transversely isotropic Fung type passive stiffness model informed by experimental measurements (Guccione *et al.*, 1991), and the Guccione model of active tension generation (Guccione *et al.*, 1993) were adopted for the model.

The Fung type transversely isotropic passive stiffness model (Guccione *et al.*, 1991), is described by the following strain energy function (W):

$$W = \frac{1}{2}C\left(e^{b_{ff}E_{ff}^2 + b_{xx}\left(E_{ss}^2 + E_{nn}^2 + E_{sn}^2 + E_{ns}^2\right) + b_{fx}\left(E_{fn}^2 + E_{nf}^2 + E_{fs}^2 + E_{sf}^2\right)} - 1\right), \quad \text{Equation 4}$$

where C is the passive stiffness coefficient, E was the Green-Lagrange Strain, with subscripts f, s and n denoting the fiber, sheet and sheet-normal directions, respectively, and b is the stiffness exponent in specific directions specified by its subscript. Stiffness parameters described in Guccione et al.'s study was simply adopted (Guccione *et al.*, 1991), parameter values are disclosed in Table 2. Stiffness parameters were assumed to be the same across all our cases, as case specific recovery of individualized stiffness parameters was not possible. Our previous studies demonstrated that minor scaling of the material stiffness parameters does not significantly affect the biomechanics and function of the heart, since stiffness was typically an order of magnitude smaller than the active tension generated by the heart (Ong *et al.*, 2020).

Active tension (P_{act}) generation of myocardium was modelled using Guccione et al.'s calcium activation model (Guccione *et al.*, 1993), where P_{act} is expressed as:

$$P_{act} = T_{0,LV}\frac{Ca_0^2}{Ca_0^2 + ECa_{50}^2}C_t, \quad \text{Equation 5}$$

where $T_{0,LV}$ describes the maximum fiber tension, which is a representation of the overall contractility and was back computed in the patient specific modelling protocol. The value of Ca_0, is described in Table 2 and ECa_{50}^2 and the sarcomere length dependent calcium sensitivity (ECa_{50}) is calculated as follows:

$$ECa_{50} = \frac{Ca_0}{\sqrt{exp[B(l - l_0)] - 1}}, \quad \text{Equation 6}$$

where B is a constant, that described the shape of peak isometric tension-sarcomere length relation, l is sarcomere length and l_0, is the sarcomere length at no tension generation.

C_t in Equation 5 is the temporal variation of the calcium activation model:

$$C_t = \frac{1}{2}(1 - \cos\omega), \qquad \text{Equation 7}$$

where ω was dependent on the cycle time, with the variation:

$$\omega = \begin{cases} \pi \dfrac{t}{t_0} \; when \; 0 \le t < t_0 \, , \\ \pi \dfrac{t - t_0 + t_r}{t_r} \; when \; t_0 \le t < t_0 + t_{r,} \\ 0 \; when \; t_0 + t_r \le t, \end{cases} \qquad \text{Equation 8}$$

where t_0 was the time to peak tension, calculated using the model specific cardiac cycle length and Mulieri et al.'s measured relationship between cardiac cycle and time to peak tension (Mulieri *et al.*, 1992). t_r, was the relaxation time and was calculated using the following equation:

$$t_r = ml + b, \qquad \text{Equation 9}$$

where m is the gradient of linear relaxation duration and b is the time intercept of linear relaxation duration, dependent on the degree of myocyte stretch.

For all models, the myocardium helix angle (HA) was assumed to vary linearly from the epicardium to endocardium, from -52° to +71° respectively (example in Figure 3B), which was the average HA configuration reported in 3 previous fetal LV tissue studies (Ohayon *et al.*, 1999; Garcia-Canadilla *et al.*, 2018; Nishitani *et al.*, 2020). Before computations, the unloaded state of the LV, or the theoretical geometry of the heart at zero LV cavity pressure, was calculated and assumed to be the stress-free condition. This was achieved via Finsberg et al.'s backward displacement method (Finsberg *et al.*, 2018): the pressure loading from the load-free state to the end diastolic state was iteratively simulated until the targeted end-diastolic pressure and volume was achieved, and at every iteration, the load-free state was adjusted by changing the pressure for an inverse of the loading deformation. The targeted end diastolic pressure was set as 5 mmHg for healthy hearts (Johnson *et al.*, 2000), but this was adjusted incrementally upwards in 1 mmHg intervals if negative pressures were encountered during early diastole. For diseased cases, end-diastolic pressure was assigned by the end-diastolic left atrium (LA) pressure, obtained by assuming a linear relationship between LA size and pressure (LA compliance) (Matsuda *et al.*, 1990). This models the abnormal LA pressurization in diseased cases.

The formal FE simulation was performed by minimizing the weak formulation of a Lagrangian functions described by Shavik et al. (Shavik *et al.*, 2018), which enforces tissue stress equilibrium, incompressibility, and a specific cavity volume to yield cavity pressure, using the Newton Solver in the FEniCS software. The boundary conditions were like that previously reported (Shavik *et al.*, 2018), with the basal plane of the LV constrained in the longitudinal direction and a weak 90 Pa spring applied to the entire epicardium at the load-free state, to simulate interactions with surrounding tissues and to constrain translational motion of the model.

A lumped parameter model (Figure 3C) was used for 1D modelling of fetal circulation and was coupled to the LV FE model. The lumped parameter model was based on Pennati et al.'s work (Pennati *et al.*, 1997; Pennati. & Fumero., 2000), but underwent minor recalibration to more recent measurements of human fetal intracardiac pressure (Johnson *et al.*, 2000), and descending aorta pulse pressure (Versmold *et al.*, 1981), as explained in our previous modelling study (Green *et al.*, 2022),

where all model parameters are given. The model is scalable to a range of gestational ages, through a series of allometric equations. The model was executed for 30 cycles, to ensure steady state was achieved.

Tuning Model for Patient Specific Match

The lumped parameter coupled FE modelling was iteratively performed by altering valve flow resistances and myocardial contractility, to best match each computational model with clinical measurements. Through this matching process, the patient-specificity of the model could be maintained, and the biomechanics parameters could be back-computed.

For healthy fetal hearts, the lumped parameter model was first scaled to the specific gestational age. Iterative FE and lumped parameter simulations were then performed while varying myocardial contractility ($T_{0,LV}$ in Equation 5), until the simulated stroke volume matched that measured from the image, thus back-computing the contractility. 60 kPa was used as the initial guess of active tension magnitude, based on the upper limit of experimental measurements of 49.9 $\pm$ 9.3 kPa of fetal myocardium at 18+4 wks+days gestation (Racca *et al.*, 2016).

For CAS-eHLHS hearts, the lumped parameter model was again scaled to the specific gestational age. The patient specific matching process, however, was more extensively performed. First, iterative simulations were performed while varying flow resistances of the AV, mitral valve (MV) inflow and MVr, until simulations matched the expected valvular pressure gradients, which were calculated from each patients clinical valvular Doppler velocities, using the simplified Bernoulli's equation. Next, iterative simulations were performed while adjusting myocardial contractility, until the simulated stroke volume matched that measured from images. A loop over the two types of iterative simulations was performed, until both valvular pressure gradients and stroke volume matched measurements from echo images. This thus allowed the back-computation of myocardial contractility.

A simple gradient descent algorithm was used to reach convergence for all iterative simulations, and parameter matches were optimized to minimize errors as much as possible, to less than 10% error. Where a satisfactory match could not be obtained, the age scaling of the lumped parameter was adjusted and the optimization process was repeated, until a match could be achieved.

Calculation of Biomechanics Characteristics

A series of biomechanics characteristics were output to evaluate the functionality of the healthy and diseased models. LV work done or the work done by the LV on ejected fluid was calculated as the area within the PV loop. Peak Systolic Myofiber Stress was calculated by taking the component of the stress tensor in the direction of the helix angle, and then performing spatial averaging over the entire myocardial volume, at the time point where pressure was maximum, as shown in Equation 10:

$$Peak\ Systolic\ Myofiber\ Stress = \frac{1}{V}\int_V \overrightarrow{f_d}\boldsymbol{\sigma}\overrightarrow{f_d}\, dV \qquad \text{Equation 10}$$

where V is is the volume of the myocardium, $\overrightarrow{f_d}$ is unit vector in the myocardial direction, and $\boldsymbol{\sigma}$ is the stress tensor at peak systole.

Principal Component and Regression Analysis

Firstly, correlation analysis was performed between peak systolic volume-averaged myocardial stress to various echo parameters. A simple linear mathematical equation was then developed for rapid computation of peak-systolic volume-averaged myocardial stress from clinically measurable echo

parameters that demonstrated with strong correlation to myocardial stress. The parameters that had a good correlation and/or were theoretically relevant to myofiber stress were, AV velocity, MVr velocity, LV longitudinal length, RV longitudinal length, LVID, RWT, EDV and SV (Note: EDV and SV were calculated by applying the half prolate ellipsoid equation to describe LV volume at EDV and ESV), as listed in Equation 11a. Principal component analysis was then used to seek modes or linear combinations of the echo parameters that best described the variability between diseased fetal cases. The resulting top three modes from the analysis described 93.05% of the cumulative proportion and are shown in Equation 11b. Then regression was performed to determine the coefficient for these modes (Equation 11c), so that a weighted sum of these modes could be used to estimate peak systolic myofiber stress. The final formulation of the principal component and regression analysis is outlined in Equation 11d.

$$\vec{V} = \begin{bmatrix} AV\ Velocity \\ MVr\ Velocity \\ LV\ Longitudinal\ Length \\ RV\ Longitudinal\ Length \\ LVID \\ RWT \\ EDV \\ SV \end{bmatrix} \qquad \text{Equation 11a}$$

$$\begin{bmatrix} \overrightarrow{PC_1} & \overrightarrow{PC_2} & \overrightarrow{PC_3} \end{bmatrix} = \begin{bmatrix} 0.3393 & -0.4374 & 0.2430 \\ 0.01739 & -0.7685 & -0.002620 \\ -0.4014 & -0.07994 & 0.4159 \\ -0.4041 & -0.2020 & 0.2223 \\ -0.4352 & 0.04481 & 0.1248 \\ 0.3460 & -0.1418 & 0.4632 \\ -0.4150 & -0.02060 & 0.2708 \\ -0.2807 & -0.3851 & -0.6443 \end{bmatrix} \qquad \text{Equation 11b}$$

$$\begin{bmatrix} a_0 & a_1 & a_2 & a_3 \end{bmatrix} = \begin{bmatrix} -24.9240 & -1.9403 & -5.5865 & -3.4160 \end{bmatrix} \qquad \text{Equation 11c}$$

$$Peak\ Systolic\ Myofiber\ Stress = a_0 + a_1\overrightarrow{PC_1} \cdot \vec{V} + a_2\overrightarrow{PC_2} \cdot \vec{V} + a_3\overrightarrow{PC_3} \cdot \vec{V} \qquad \text{Equation 11d}$$

Receiver Operating Characteristic (ROC) Analysis

To determine which pre-FAV image-based characteristic had the greatest capability in distinguishing BV versus UV outcomes, ROC analysis was performed on retrospective images (n=37). The 9 cases used to develop the mathematical equation to compute myocardial stress were used here as well, as part of the 37 samples. This was appropriate as the equation was developed only to approximate myocardial stress, and this was done without any reference to outcomes of the cases. Outcomes data was only used in the ROC analysis. Samples with incomplete datasets were not included here. The analysis was performed on parameters within this study, and for RV/LV longitudinal length ratio and estimated peak LV pressure, which were identified by Tulzer et al. (Tulzer *et al.*, 2022*a*) and Friedman et al. (Friedman *et al.*, 2018) as promising pre-FAV parameters for indicating post-FAV outcomes.

Statistical Analysis

Z-scores for echo measurements parameters were computed using healthy population data from Luewan et al. for LVID and PWT (Luewan *et al.*, 2011), from Devore et al. for LV and RV longitudinal

length, end-diastolic volume (EDV), stroke volume and ejection fraction (DeVore *et al.*, 2017; Devore *et al.*, 2019) and Chen et al. for ascending aorta diameter dimensions (Chen *et al.*, 2022). For biomechanics parameters from computational outputs, no population data is currently available in literature, to eliminate the age dependent variation, therefore, when a computational parameter showed a trend of variability with age, it was normalized with the regression line of our healthy cohort before being analysed.

All results are reported as mean and standard deviation. The Mann-Whitney U test performed on all data comparisons due to small sample sizes (except for the ROC analysis where the DeLong test was used). Statistical significance assumed when $P < 0.05$. To estimate the effect size of differences in specific parameters between the BV and UV groups the Cohen's D value was calculated as,

$$d = \frac{\bar{x}_{BV} - \bar{x}_{UV}}{s_p} \times corr \qquad \text{Equation 12}$$

where $\bar{x}$, is the mean value of the parameter for the UV or BV group as indicated by the subscript, s_p is the pooled standard deviation and $corr = 0.7839$ and is the correction factor for when $n < 50$.

RESULTS

Echocardiography Anatomic and Functional Measurements

Echocardiography cardiac anatomic and functional measurements for pre-FAV and healthy control hearts are shown in Figure 4. Pre-FAV peak valvular velocity measurements (Figure 4A-C) showed no statistical significance between the BV and UV disease sub-groups, although both AV and MV antegrade velocities were substantially higher than healthy hearts. Both BV and UV disease sub-groups had elevated EDV Z scores from healthy controls, but the difference was only significant between BV and healthy groups, and not between BV and UV groups (Figure 4D). Both BV and UV groups had significantly lower stroke volume and ejection fraction Z scores than healthy groups but again, there was no significant difference between BV and UV groups (Figure 4E-F). The BV group had significantly higher LV and RV longitudinal length than controls (Figure 4G-H), and although BV LV longitudinal length was generally higher than the UV group, the difference was not significant. Similarly, the BV group generally had higher LVID (Figure 4J), lower RWT (Figure 4M), and higher aspect ratio (Figure 4K), than the UV group and healthy controls, but again significance was found only between the BV and control group. No significance was observed across all groups in RV/LV length ratio (Figure 4I) and PWT (Figure 4L). For ascending aorta diameter Z score, healthy patient specific data was not available for ascending aorta calculations and therefore the standard deviation of normative data has been included in Figure 4N (Chen *et al.*, 2022). No statistical significance was found between BV and UV groups, but both BV and UV groups were significantly greater than healthy controls. In terms of strains, both BV and UV groups were significantly smaller than healthy controls, but again, no significance was observed between the BV and UV groups (Figure 4O-P).

Overall, the data demonstrated that diseased hearts were larger than healthy hearts and had lower strains and stroke volume. Between the BV and UV groups, BV hearts tended to have larger average dimensions and higher average strains than UV hearts. However, there were consistently significant overlaps in measurements between the two groups, suggesting that it may not be easy to distinguish between the two groups with echo measurements alone.

Image-Based Simulations of Cardiac Biomechanics

The iterative FE modelling optimization process produced percentage error between simulation parameters and image-measured parameters of 2.55 ±3.56%, 6.43 ±4.20%, and 4.80 ±3.94% for stroke

volume, AV pressure gradient and MVr pressure gradient respectively. MV pressure gradients were minimized to within 0.7 mmHg of the image-based value. Detailed data demonstrating this is given in Supplementary Data file at https://doi.org/10.6084/m9.figshare.24793494.

Figure 5 shows representative results from the image-based FE simulations, showing that the resulting pressure-volume (P-V) loops and spatially averaged myofiber stress over the cardiac cycle were reasonably physiologic.

Peak LV pressure was known to increase with gestational age according to previous invasive measurements (Johnson *et al.*, 2000), shown in Figure 6A. From the trends of computed results, LV work done (the area within the P-V loop), and myocardial contractility of healthy models also increased with gestational age from regression analysis (Figure 6B and D). To account for the age dependency of these biomechanics' parameters, the parameters were normalized by the expected value of a healthy heart of the same age from the regression analysis, before comparisons between groups were performed. Literature data was used for normalization in Figure 6A because it has more samples and is more robust, but our healthy cohort data was used for normalization in Figure 6B and D because no such literature data exists. For peak systolic myocardial stress in the myofiber direction (Figure 6C), it appeared to have little change over age, and as such, no normalization was done.

From the normalized quantifications, diseased hearts were found to have generally higher LV pressures compared to the healthy controls and the UV group, but no statistical significance was found (Figure 6E). Diseased hearts had significantly lower work done than healthy hearts, and the BV hearts produced higher work than the UV hearts, but no significance was found between BV and UV groups (Figure 6F). In terms of peak systolic myofiber stress, UV hearts had very similar values to healthy hearts, and the BV hearts had a drastic elevation (more than two-fold), which was significantly higher than both the UV and healthy groups, with no data overlap between the groups (Figure 6G). For myocardial contractility, both diseased groups were significantly lower than healthy controls, and a significant difference was observed between BV and UV groups. However, there was some overlap between the UV and BV data.

Overall, the data demonstrated that diseased hearts had significantly altered biomechanics, including elevated cavity pressures and decreased circulatory work done and lower myocardial contractility compared to healthy hearts. Further, BV but not UV LVs experienced higher myocardial stresses than controls. Between the BV and UV groups, both contractility and peak systolic myofiber stress were significantly different. The difference in peak systolic myofiber stress between BV and UV hearts was especially large with no overlap between the two groups. This was thus potentially a good parameter for distinguishing the two groups, for predicting FAV outcomes.

Effect Size of Parameter Differences Between UV and BV Groups

To determine which of the parameters investigated had stronger ability to distinguish between UV and BV groups, we computed the Cohen's D standardized mean difference (Figure 7) for all CAS-eHLHS cases modelled. The Cohen's D value quantified how different parameter values between the UV and BV groups were. Results showed that myofiber stress had the highest Cohen's D, which was much higher than Cohen's D for any other parameters. This was followed by echo-measured ventricular size parameters such as LV longitudinal length and LVID, which were close to the biomechanics parameters, normalized work done and contractility.

Relationship Between Echocardiographic Parameters and Biomechanics Parameters

To understand the dependencies of the peak systolic myofiber stress, we performed correlation analysis between stress and echo parameters. We found that myocardial stress had a good positive

correlation with LV size parameters (EDV, longitudinal length, SV and LVID), and MVr, and a good negative correlation with RWT (Table 8A). The correlations are logical from the theoretical standpoint. Myocardial stress was determined via a force balance between the cavity blood pressure and tensile forces in the myocardial walls, and was thus higher with greater systolic pressure, which was the driver of regurgitation. Myofiber stress thus correlated positively with MVr. Further, myocardial wall stresses could be approximated by myocardial wall forces divided by cross-sectional area, which was determined by wall thickness. Myofiber stress thus correlated negatively with RWT. The relationship between cavity pressure and wall tension was further governed by the shape of the LV chamber, as could be illustrated by the hoop stress theory, which stated that larger chambers had higher wall tension. Myofiber stress thus correlated positively with LV size. Finally, peak AV velocity was included, as from a theoretical perspective the value of peak AV velocity indicates degree of aortic stenosis. These theories thus suggested that it is possible to derive a parameter that can be easily calculated with measurable echo parameters to theoretically represent peak systolic myofiber stress. This will enable fast and easy estimation of myofiber stress from echo scans without a need for time consuming simulations, for the prediction of FAV outcomes.

These parameters were used to develop an empirical equation for rapid computation of stress from clinical measurements, via principal component and regression analyses. Combining all facets of the principal component analysis with regression coefficients generated Equation 13. The resulting equation for estimating peak systolic myofiber stress had a good correlation with the actual peak systolic myofiber stress from FE simulations, as demonstrated by Figure 8B.

$$\begin{aligned} &Estimated\ Peak\ Systolic\ Myofiber\ Stress \\ &\quad = -24.9240 + 0.9550V_1 + 4.2687V_2 - 0.1952V_3 + \\ &1.1530V_4 + 0.1677V_5 - 1.4611V_6 - 0.004771V_7 + 4.8968V_8 \end{aligned} \qquad \text{Equation 13}$$

Where V_1 to V_8 are echo parameters as given in Equation 11a.

Possible Post-FAV Outcome Predictors, A Retrospective Analysis

ROC analysis was performed to determine the ability of peak systolic myofiber stress, estimated via Equation 13, in classifying BV versus UV outcomes, to compare it with that of other known image-based pre-FAV predictors (Friedman *et al.*, 2018; Tulzer *et al.*, 2022*a*), and with individual parameters within Equation 13. Detailed echo measurements used for computing myofiber stress via Equation 13 are provided in the Supplementary Data Spreadsheet at https://doi.org/10.6084/m9.figshare.24793494. The results show estimated peak systolic myofiber stress to have the largest area under the curve (AUC) of 0.91 and therefore the greatest capability in distinguishing BV versus UV outcomes (Figure 9). The next best performing parameters were LV longitudinal length Z score (AUC=0.84) and EDV Z score (AUC=0.83). The approach of estimating peak myofiber stress was significantly better at distinguishing BV versus UV outcomes than RWT, MVr velocity, estimating pressure and AV velocity.

DISCUSSION

We performed a retrospective analysis of CAS-eHLHS fetal hearts to identify pre-FAV parameters that have a high likelihood of having the ability to predict UV versus BV outcomes, after FAV intervention. To do this, we investigated differences in various parameters between UV and BV groups. Our study is different from previous such works in that we performed advanced patient-specific biomechanics simulations to obtain biomechanics parameters, to add on to echocardiographic parameters in our analysis. Our simulations enabled careful back-computation of the myocardial contractility and LV pressures, while adhering to echocardiographic image features and detailed

biomechanics formulations, and it provided information on myocardial stresses, which are not measurable clinically. Importantly, our results showed that myocardial stress is uniquely large in the BV group and is potentially a better parameter for predicting UV versus BV outcomes than all currently proposed clinical parameters.

Overall, our measurements agreed well with previous investigations on differences between UV and BV groups. Firstly, our data showed that BV groups had generally higher mean circumferential and longitudinal strains than UV groups, which were significantly lower than control groups. Ishii et al. (Ishii *et al.*, 2014) reported in a larger cohort study (n=57) that there were similarly diminished strain magnitudes in diseased hearts, and found significant differences between UV and BV groups for circumferential strains in 1 out of 6 segments of the LV and for longitudinal strains in 3 out of 6 segments of the LV. In our study, however, as our sample sizes are smaller (n=15), UV-versus-BV statistical significances were not found.

Secondly, our data showed that the BV group had higher EDVs (Figure 4D), LV longitudinal lengths (Figure 4G), RV longitudinal lengths (Figure 4H) and LVIDs (Figure 4J) than the UV group, but differences were not statistically significant. This aligns with previous studies, which analyzed retrospective data and found cases that went on to be born as BV after intervention generally had larger LV long axis Z scores (Friedman *et al.*, 2018) and larger left heart structures (including, aortic valve Z score, LV short axis Z score and LV long axis Z score) (McElhinney *et al.*, 2009) at the pre-FAV time point. Again, our small sample size had likely prevented a statistical significance, but our data generally corroborated with literature on the direction of the UV versus BV differences.

Thirdly, our simulation results showed LV pressures were generally higher in BV hearts compared to UV hearts, but differences were not significant. Friedman et al. and McElhinney et al. estimated LV pressure from valve Doppler measurements and found that BV cases had significantly higher LV pressures compared with UV cases at the time of intervention (McElhinney *et al.*, 2009; Friedman *et al.*, 2018), which corroborated our observations. Our data thus corroborated Friedman et al. and McElhinney et al.'s, and the lack of significance could again be attributable to our small sample size. However, we noted that Friedman et al. and McElhinnery et al. did not factor in pressure variation with gestational age (Johnson *et al.*, 2000) when analyzing LV pressure calculations, as we did. When we switched to an analysis of LV pressures without the age-normalization (Supplementary Data file at https://doi.org/10.6084/m9.figshare.24793494), we found that differences between UV and BV groups were larger than if normalization was done (lower P value).

Our main finding was that peak systolic myofiber stress was the best pre-FAV parameter to distinguish between UV and BV cases, and this outperformed all other parameters, including several that were found to have good predictive values in previous studies (Ishii *et al.*, 2014; Friedman *et al.*, 2018; Tulzer *et al.*, 2022*a*). For example, Tulzer et al. showed that RV-to-LV length ratio had strong predictive influence (Tulzer *et al.*, 2022*a*), Friedman et al. reported a high probability of a BV outcome in cases where peak LV pressure was >47 mmHg and ascending aorta Z-score was ≥0.57 (Friedman *et al.*, 2018), while Ishii et al. reported higher LV longitudinal and circumferential strains in BV compared to UV cases (Ishii *et al.*, 2014). We made the comparison of these individual parameters to peak systolic myofiber stress and found that the latter still performed better. A limitation of our study is that sample sizes were smaller than previous reports, nonetheless, given that the effect size of myofiber stress is much higher than other parameters Figure 7, results are likely to repeatable with larger samples. Thus, myofiber stress has a good potential of enhancing predictions of UV versus BV outcomes. It can be used to enhance predictive framework such as the CART analysis proposed by Tulzer et al., which uses a

combination of RV-to-LV length ratio, LV pressure (calculated from peak MVr velocity) and gestational age for prediction (Tulzer *et al.*, 2022*a*).

We believe that there are physiological explanations for why hearts with stronger contractility and higher stresses are likely to reach a BV outcome instead of a UV outcome. Stronger hearts are likely to support better contractile deformations after FAV intervention, providing better biomechanical stimuli for growth of the LV and thus supporting better growth and development before birth. Further, higher myocardial stresses in BV cases suggested that the myocardium in these cases resisted pathological hypertrophy and dilation remodeling despite high tissue stresses, while retaining a strong functional ability to generate pumping pressures. This might suggest that the myocardium is healthier and could elicit better growth and remodeling responses after intervention. Generally, our results suggest that biomechanically "stronger" LVs are more likely to respond positively to FAV, by progressing to a successful BV outcome at one year of age.

Our results suggest that biomechanical simulations of fetal hearts can improve predictive capabilities of outcomes, and this is likely useful for clinical decisions. However, presently, biomechanical simulations are computationally expensive, and involve multiple processing steps including the computational reconstruction of the heart's structure and motion. We have thus proposed a simplified equation to quickly estimate the peak systolic myocardial stress from echo parameters with ease, as shown in Equation 13. Although this equation will not be as accurate as the FE simulations, we showed in Figure 8b that it retained its ability to clearly distinguish BV and UV groups. The equation can be updated in future for accuracy when more data becomes available, or to reduce the number of dependent parameters to reduce error propagation. There is also potential for using Physics-Informed Neural Networks to achieve accurate, real-time estimations of myocardial stresses (Buoso *et al.*, 2021).

When we performed validation on 37 CAS-eHLHS cases, we found that the estimated peak systolic myofiber stress parameter remained the best predictor of UV versus BV post-FAV outcomes, judging from its high AUC in the ROC analysis. Statistical significance, however, was observed only with some of the parameters compared to, likely due to the small sample size. It is further is likely that errors involved in estimating myocardial stresses via a simple linearized equation based on a small sample cohort had resulted in some reduction of predictive performance. In the future, refinement of Equation 13 should be performed, which could improve the statistical significance. Longer term biomechanics simulations may be possible in real-time via machine learning, particularly with physics informed neural networks, which could resolve this issue altogether. We believe that such future work is warranted. From the ROC analysis, a potentially useful peak systolic myofiber threshold can be obtained for use in predictions. The threshold of stress = 17.4 kPa provides 100% sensitivity, and approximately 73% specificity (thus correctly predicting all BV cases), the threshold of stress = 26.1 kPa provides approximately 41% sensitivity and 100% specificity (thus correctly predicting all UV cases), while the threshold of stress = 17.4 kPa corresponds to the highest accuracy (average of sensitivity and selectivity weighted by prevalence), which correctly predicts 100% of BV cases and approximately 73% of UV cases. Presently, it is unclear which is the most clinically beneficial threshold to use, and further risk versus benefit analysis should be conducted. For example, recent thought about FAV is that even for UV outcomes, the FAV could have reduced disease severity and improved survival benefits, and such a notion warrants further studies.

There are several limitations of this study. Firstly, our sample size is small, and future studies with larger sample sizes are likely to enhance the current analysis and produce positive refinement to our prediction model in Equation 13. Secondly, all CAS-eHLHS patients analyzed in the study had already been selected for FAV intervention and the sample size was small due to limited data availability, which

imposed bias, it would be recommended to widen the study, to help mitigate this limitation. Thirdly, our biomechanics computations required idealizations, such as the assumption of the same HA spatial variability configuration, lumped parameters model values, and myocardial stiffness for all cases. Also, during the optimisation loops, the best possible match with imaged parameters was obtained, but some match errors remained. Finally, it must be acknowledgement that CAS-eHLHS data was only obtained from 1 institute and BV or UV outcome largely depends on the institutional experience and management algorithm, which is not standardized between centers.

CONLCUSIONS

Biomechanics parameters, including peak systolic myofiber stress and back-computed myocardial contractility seemed to be promising metrics to differentiate between UV and BV cases. Importantly, peak-systolic myofiber stress had a uniquely large difference between UV and BV cases, suggesting that it has the potential of being a better indicator of UV versus BV outcome than all other current clinical measurements. A simplified equation for estimating myocardial stress showed that this parameter has better predictive capabilities compared to echo measurements. We speculate that this parameter can be helpful in clinical evaluation for a more accurate patient selection for FAV.

ADDITIONAL INFORMATION

Data Availability Statement

FE computational codes are available at https://github.com/WeiXuanChan/heartFEM. Detailed data used to plot Figures 4, 6, 7 and 9 are available in the Supplementary Spreadsheet at https://doi.org/10.6084/m9.figshare.24793494

Competing Interests

The authors have no conflict of interest to declare.

Author Contributions

Laura Green – Designed research, developed methodologies, performed simulations, analyzed data, interpreted data, prepared manuscript, and vetted manuscript.

Dr Wei Xuan Chan – Designed research, developed modelling formulation, interpreted data, vetted manuscript.

Indumita Prakash – Performed simulations and analyzed data.

Dr Andreas Tulzer – Performed clinical intervention, collected clinical data, analyzed data, interpreted data, vetted manuscript.

Dr Gerald Tulzer – Performed clinical intervention, collected clinical data, interpreted data, vetted manuscript.

Dr Choon Hwai Yap – Designed research, developed methodologies, analyzed data, interpreted data, prepared manuscript, vetted manuscript.

Artificial Intelligence Generated Content (AIGC)

No generative artificial intelligence tools were used in the preparation of this manuscript.

Funding

The Study was supported by Imperial College PhD scholarship (Green), and BHF Centre of Research Excellence grant (RE/18/4/34215, Chan).

REFERENCES

Beattie MJ, Friedman KG, Sleeper LA, Lu M, Drogosz M, Callahan R, Marshall AC, Prosnitz AR, Lafranchi T, Benson CB, Wilkins-Haug LE & Tworetzky W (2020). Late gestation predictors of a postnatal biventricular circulation after fetal aortic valvuloplasty. *Prenat Diagn* **41,** 479–485.

Buoso S, Joyce T & Kozerke S (2021). Personalising left-ventricular biophysical models of the heart using parametric physics-informed neural networks. *Med Image Anal* **71,** 1–11.

Chen F, Zeng S, Yi A, Chen L, Zhou D, Liu Y & Yao L (2022). Z-score model of foetal ascending aorta diameter distensibility. *Front Cardiovasc Med* **9,** 1–7.

DeVore GR, Klas B, Satou G & Sklansky M (2017). Evaluation of the right and left ventricles: An integrated approach measuring the area, length, and width of the chambers in normal fetuses. *Prenat Diagn* **37,** 1203–1212.

Devore GR, Klas B, Satou G & Sklansky M (2019). Evaluation of fetal left ventricular size and function using speckle-tracking and the simpson rule. *Journal of Ultrasound in Medicine* **38,** 1209–1221.

Dewan S, Krishnamurthy A, Kole D, Conca G, Kerckhoffs R, Puchalski MD, Omens JH, Sun H, Nigam V & McCulloch AD (2017). Model of human fetal growth in hypoplastic left heart syndrome: Reduced ventricular growth due to decreased ventricular filling and altered shape. *Front Pediatr* **5,** 1–15.

Finsberg H, Xi C, Tan J le, Zhong L, Genet M, Sundnes J, Lee LC & Wall ST (2018). Efficient estimation of personalized biventricular mechanical function employing gradient-based optimization. *Int J Numer Method Biomed Eng* **34,** 1–20.

Friedman KG, Sleeper LA, Freud LR, Marshall AC, Godfrey ME, Drogosz M, Lafranchi T, Benson CB, Wilkins-Haug LE & Tworetzky W (2018). Improved technical success, postnatal outcome and refined predictors of outcome for fetal aortic valvuloplasty. *Ultrasound in Obstetrics and Gynecology* **52,** 212–220.

Garcia-Canadilla P, Dejea H, Bonnin A, Balicevic V, Loncaric S, Zhang C, Butakoff C, Aguado-Sierra J, Vázquez M, Jackson LH, Stuckey DJ, Rau C, Stampanoni M, Bijnens B & Cook AC (2018). Complex Congenital Heart Disease Associated With Disordered Myocardial Architecture in a Midtrimester Human Fetus. *Circ Cardiovasc Imaging* **11,** 1–10.

Gardiner HM et al. (2016). Natural history of 107 cases of fetal aortic stenosis from a European multicenter retrospective study. *Ultrasound in Obstetrics and Gynecology* **48,** 373–381.

Green L, Chan WX, Ren M, Mattar C, Chuan L, Choon L & Yap H (2022). The dependency of fetal left ventricular biomechanics function on myocardium helix angle configuration. *Biomech Model Mechanobiol*; DOI: 10.1007/s10237-022-01669-z.

Guccione JM, McCullock AD & Waldman LK (1991). Passive material properties of intact ventricular myocardium determined from a cylindrical model. *J Biomech Eng* **113,** 42–55.

583 Guccione JM, Waldman LK & McCulloch AD (1993). Mechanics of active contraction in cardiac muscle:
584 Part II—cylindrical models of the systolic left ventricle. *J Biomech Eng* **115,** 82–90.

585 Ishii T, McElhinney DB, Harrild DM, Marcus EN, Sahn DJ, Truong U & Tworetzky W (2014). Ventricular
586 strain in fetuses with aortic stenosis and evolving hypoplastic left heart syndrome before and after
587 prenatal aortic valvuloplasty. *Fetal Diagn Ther* **35,** 18–26.

588 Johnson P, Maxwell DJ, Tynan MJ & Allan LD (2000). Intracardiac pressures in the human fetus. *Heart* **84,**
589 59–63.

590 Li Y, Sun J, Tang CK & Shum HY (2004). Lazy snapping. *ACM Trans Graph*303–308.

591 Luewan S, Yanase Y, Tongprasert F, Srisupundit K & Tongsong T (2011). Fetal cardiac dimensions at 14-
592 40 weeks' gestation obtained using cardio-STIC-M. *Ultrasound in Obstetrics and Gynecology* **37,**
593 416–422.

594 Mäkikallio K, McElhinney DB, Levine JC, Marx GR, Colan SD, Marshall AC, Lock JE, Marcus EN &
595 Tworetzky W (2006). Fetal aortic valve stenosis and the evolution of hypoplastic left heart
596 syndrome: Patient selection for fetal intervention. *Circulation* **113,** 1401–1405.

597 Matsuda Y, Toma Y, Matsuzaki M, Moritani K, Satoh A, Shiomi K, Ohtani N, Kohno M, Fujii T, Katayama K,
598 Matsuda M & Kusukawa R (1990). Change of left atrial systolic pressure waveform in relation to
599 left ventricular end-diastolic pressure. *Circulation* **82,** 1659–1667.

600 McElhinney DB, Marshall AC, Wilkins-Haug LE, Brown DW, Benson CB, Silva V, Marx GR, Mizrahi-Arnaud
601 A, Lock JE & Tworetzky W (2009). Predictors of technical success and postnatal biventricular
602 outcome after in utero aortic valvuloplasty for aortic stenosis with evolving hypoplastic left heart
603 syndrome. *Circulation* **120,** 1482–1490.

604 Mulieri LA, Hasenfuss G, Leavitt B, Allen PD & Alpert NR (1992). Altered myocardial force-frequency
605 relation in human heart failure. *Circulation* **85,** 1743–1750.

606 Nishitani S, Torii N, Imai H, Haraguchi R, Yamada S & Takakuwa T (2020). Development of helical
607 myofiber tracts in the human fetal heart: Analysis of myocardial fiber formation in the left ventricle
608 from the late human embryonic period using diffusion tensor magnetic resonance imaging. *J Am*
609 *Heart Assoc*; DOI: 10.1161/JAHA.120.016422.

610 Ohayon J, Usson Y, Jouk PS & Cai H (1999). Fibre orientation in human fetal heart and ventricular
611 mechanics: A small perturbation. *Comput Methods Biomech Biomed Engin* **2,** 83–105.

612 Ong CW, Ren M, Wiputra H, Mojumder J, Chan WX, Tulzer A, Tulzer G, Buist ML, Mattar CNZ, Lee LC &
613 Yap CH (2020). Biomechanics of Human Fetal Hearts with Critical Aortic Stenosis. *Ann Biomed Eng*;
614 DOI: 10.1007/s10439-020-02683-x.

615 Pennati G, Bellotti M & Fumero R (1997). Mathematical modelling of the human foetal cardiovascular
616 system based on Doppler ultrasound data. *Med Eng Phys* **19,** 327–335.

617 Pennati. G & Fumero. R (2000). Scaling approach to study the changes through the gestation of human
618 fetal cardiac and circulatory behaviors. *Ann Biomed Eng* **28,** 442–452.

Pickard SS, Wong JB, Bucholz EM, Newburger JW, Tworetzky W, Lafranchi T, Benson CB, Wilkins-Haug LE, Porras D, Callahan R & Friedman KG (2020). Fetal Aortic Valvuloplasty for Evolving Hypoplastic Left Heart Syndrome: A Decision Analysis. *Circ Cardiovasc Qual Outcomes* **13,** 32–41.

Prosnitz AR, Drogosz M, Marshall AC, Wilkins-Haug LE, Benson CB, Sleeper LA, Tworetzky W & Friedman KG (2018). Early hemodynamic changes after fetal aortic stenosis valvuloplasty predict biventricular circulation at birth. *Prenat Diagn* **38,** 286–292.

Racca AW, Klaiman JM, Pioner JM, Cheng Y, Beck AE, Moussavi-Harami F, Bamshad MJ & Regnier M (2016). Contractile properties of developing human fetal cardiac muscle. *Journal of Physiology* **594,** 437–452.

Ren M, Chan WX, Green L, Armstrong AK, Tulzer A, Tulzer G, Buist ML & Yap CH (2023). Contribution of Ventricular Motion and Sampling Location to Discrepancies in 2D versus 3D Fetal Ventricular Strain Measures. *Journal of the American Society of Echocardiography*; DOI: 10.1016/j.echo.2022.12.024.

Shavik SM, Jiang Z, Baek S & Lee LC (2018). High spatial resolution multi-organ finite element modeling of ventricular-arterial coupling. *Front Physiol*; DOI: 10.3389/fphys.2018.00119.

Shavik SM, Wall S, Sundnes J, Guccione JM, Sengupta P, Solomon SD, Burkhoff D & Lee LC (2021). Computational Modeling Studies of the Roles of Left Ventricular Geometry, Afterload, and Muscle Contractility on Myocardial Strains in Heart Failure with Preserved Ejection Fraction. *J Cardiovasc Transl Res* **14,** 1131–1145.

Tulzer A, Arzt W, Gitter R, Sames-Dolzer E, Kreuzer M, Mair R & Tulzer G (2022*a*). Valvuloplasty in 103 fetuses with critical aortic stenosis: outcome and new predictors for postnatal circulation. *Ultrasound in Obstetrics and Gynecology* **59,** 633–641.

Tulzer A, Arzt W, Scharnreitner I, Hochpoechler J, Bauer C & Tulzer G (2022*b*). Complications associated with fetal cardiac interventions – prevalence and management: experience from 213 procedures. *Fetal Diagn Ther*; DOI: 10.1159/000527121.

Tulzer G & Arzt W (2013). Fetal cardiac interventions: Rationale, risk and benefit. *Semin Fetal Neonatal Med* **18,** 298–301.

Versmold HT, Kitterman JA, Phibbs RH, Gregory GA & Tooley WH (1981). Aortic blood pressure during the first 12 hours of life in infants with birth weight 610 to 4,220 grams. *Pediatrics* **67,** 607–613.

Wiputra H, Chan WX, Foo YY, Ho S & Yap CH (2020). Cardiac motion estimation from medical images: a regularisation framework applied on pairwise image registration displacement fields. *Sci Rep*; DOI: 10.1038/s41598-020-75525-4.

Wisneski AD, Wang Y, Deuse T, Hill AC, Pasta S, Sack KL, Yao J & Guccione JM (2020). Impact of Aortic Stenosis on Myofiber Stress: Translational Application of Left Ventricle-Aortic Coupling Simulation. *Front Physiol* **11,** 1–8.

FIGURE LEGENDS

Abstract Figure 1. We conducted image-based patient-specific modelling of left ventricular biomechanics of fetuses with aortic stenosis undergoing valvuloplasty. A biomechanics parameters calculated, peak systolic myofiber stress, showed exceptionally high Cohen's D values between cases with good versus bad outcomes (functionally biventricular versus single ventricular at birth), suggesting robust predictive power.

Figure 1. All reconstructed cardiac geometries used in this study. [Top row] Models that went on to be funtionally BV at birth. [Middle row] Models that went on to be funtioncally UV at birth. [Bottom row] Healthy models. Scale bar shown in the top left.

Figure 2. [Top row] Example of patient specific reconstructed LV geometries for one diseased case with BV outcome, with UV outcome and a healthy case. Geometries to scale, scale bar shown under H3. [Middle row] Reconstructed geometries superimposed onto associated echo image, green outline highlighting geometry proportion close to current image plane. [Bottom row] Volume over time variation of each geometry output from cardiac motion estimation methods.

Figure 3. [A] Example of mesh applied to H3. [B] Example of fibers applied to H3, with negative fiber angle at epicardial surface and linear transmural variation to positive fiber angle at endocardial surface. (C) Schematic of lumped parameter model with H3 geometry. Note, AA: ascending aorta, AO1: aortic arch, AO2: thoracic descending aorta, AO3: abdominal descending aorta, AO4: femoral bifurcation, BR: brain, CA: cerebral arteries, HE: liver, INTE: intestinal circulation, IVC: inferior vena cava, KID: kidney, LA: left atrium, LEG: lower limbs, LUNG: lungs, LV: left ventricle, PA1: main pulmonary artery, PA2: pulmonary arteries, PLAC: placenta, RA: right atrium, RV: right ventricle, SVC: superior vena cava, UB: upper body, UV: umbilical vein. Figure adapted from published work (Pennati et al., 1997; Pennati. & Fumero., 2000).

Figure 4. Imaged-based measurements overlayed onto mean and standard deviation bar plots, for the BV and UV diseased groups, with data for healthy controls included where appropriate. Mann-Whitney U test performed on all data comparisons; statistical significance assumed when $p < 0.05$, indicated by (*) and (n.s.) denotes no significance. Sample sizes were n=5 for BV, n=4 for UV and n=6 for healthy controls. For ascending aorta diameter, literature data was used (Chen *et al.*, 2022) as measurements could not be clearly obtained from some of our images.

Figure 5. Computational biomechanics outputs for case 2 in the BV group (BV2), case 2 in the UV group (UV2) and case 3 in the healthy group (H3).

Figure 6. Biomechanical parameters output from FE simulations for the BV (n=5) and UV (n=4) diseased groups and healthy controls (n=6). [A-D] Parameters plotted with respect to gestational age. The expected normative values (dotted line) were obtained from measurements by Johnson et al. (Johnson et al., 2000) for [A], and from regression of our healthy control data for [B-D], B key applicable for C and D also. [E-H] The same biomechanics parameters after normalization, by the expected normative values for the matching gestational age, expressed as data points superimposed on mean and standard deviation bar plots. Mann-Whitney U test performed on all data comparisons; statistical significance assumed when $p < 0.05$, indicated by (*) and (n.s.) denotes no significance.

Figure 7. Cohen's D values of various parameters to describe the ability of parameters to predict intervention outcome. Sample sizes were n=5 for BV, n=4 for UV and n=6 for healthy controls.

Figure 8. [A] Relationship between peak systolic myofiber stress and various metrics of LV size. [B] Peak systolic myofiber stress value estimated using Equation 13, compared with computed peak systolic myofiber stress via FE modelling.

Figure 9. ROC curves computed from retrospective data (n=37) for the individual classes of Equation *13*, estimated peak systolic myofiber stress and literature-based pre-FAV predictors of post-FAV outcomes. AUC values for each ROC included in key and the DeLong test was used to calculate the p value of each parameter with estimated peak systolic myofiber stress; statistical significance assumed when $p < 0.05$, indicated by (*) and (n.s.) denotes no significance.

TABLES

Table 1. Patient characteristics of CAS-eHLHS cases before intervention. In diseased cases age, is the fetal age at the pre-FAV scans, which generally occurs 1-3 days before FAV intervention.

Case	Postnatal Circulation	Age (wks+days)	Multiple FAVs	Bradycardia	Pericardial Effusion	LV Thrombus	Hydrops	Postnatal Procedures
BV1	BV	24+6	N	Y	N	N	N	Dil.
BV2	BV	29+0	Y	N	N	N	Y	RK
BV3	BV	29+3	N	N	N	N	N	RK
BV4	BV	29+6	N	Y	N	N	N	N/A
BV5	BV	30+1	N	N	N	N	N	-
UV1	UV	22+4	N	N	N	Y	N	NW
UV2	UV	24+6	N	Y	N	N	N	NW
UV3	UV	27+2	N	N	N	N	N	NW
UV4	UV	29+1	Y	N	N	N	N	NW, RK, Conv.
H1	-	21+2	-	-	-	-	-	-
H2	-	21+3	-	-	-	-	-	-
H3	-	21+4	-	-	-	-	-	-
H4	-	24+0	-	-	-	-	-	-
H5	-	28+0	-	-	-	-	-	-
H6	-	32+0	-	-	-	-	-	-

Y - yes, N - no, Dil – balloon dilation of the AV, RK - Ross-Kono procedure, NW - Norwood Procedure, Conv - BV to UV conversion. N/A – no procedure as parents chose comfort care at an alternative centre; procedure planned for this patient was Ross-Konno surgery, with patient believed to progress to a BV outcome classification, therefore, for the purpose of this study the patient was classified as BV.

Table 2. Finite element modelling parameters required for both the passive and active description of the myocardium.

Parameter	Symbol	Unit	Value
Passive stiffness coefficient	C	Pa	200
Stiffness coefficient in fiber direction	b_{ff}	-	29.9
Stiffness coefficient in sheet and sheet normal direction	b_{xx}	-	13.3
Stiffness coefficient in shear directions	b_{fx}	-	26.6
Shape of peak isometric tension-sarcomere length relation	B	μm−1	4.75
Sarcomere length under no active tension	l_0	μm	1.58

Relaxed sarcomere length	l_r	μm	1.85
Time intercept of linear relaxation duration with sarcomere length	b	ms	-800
Gradient of linear relaxation duration with sarcomere length relaxation	m	msμm−1	524
Maximum intracellular calcium concentration	Ca_0	μM	4.35

716

717

718

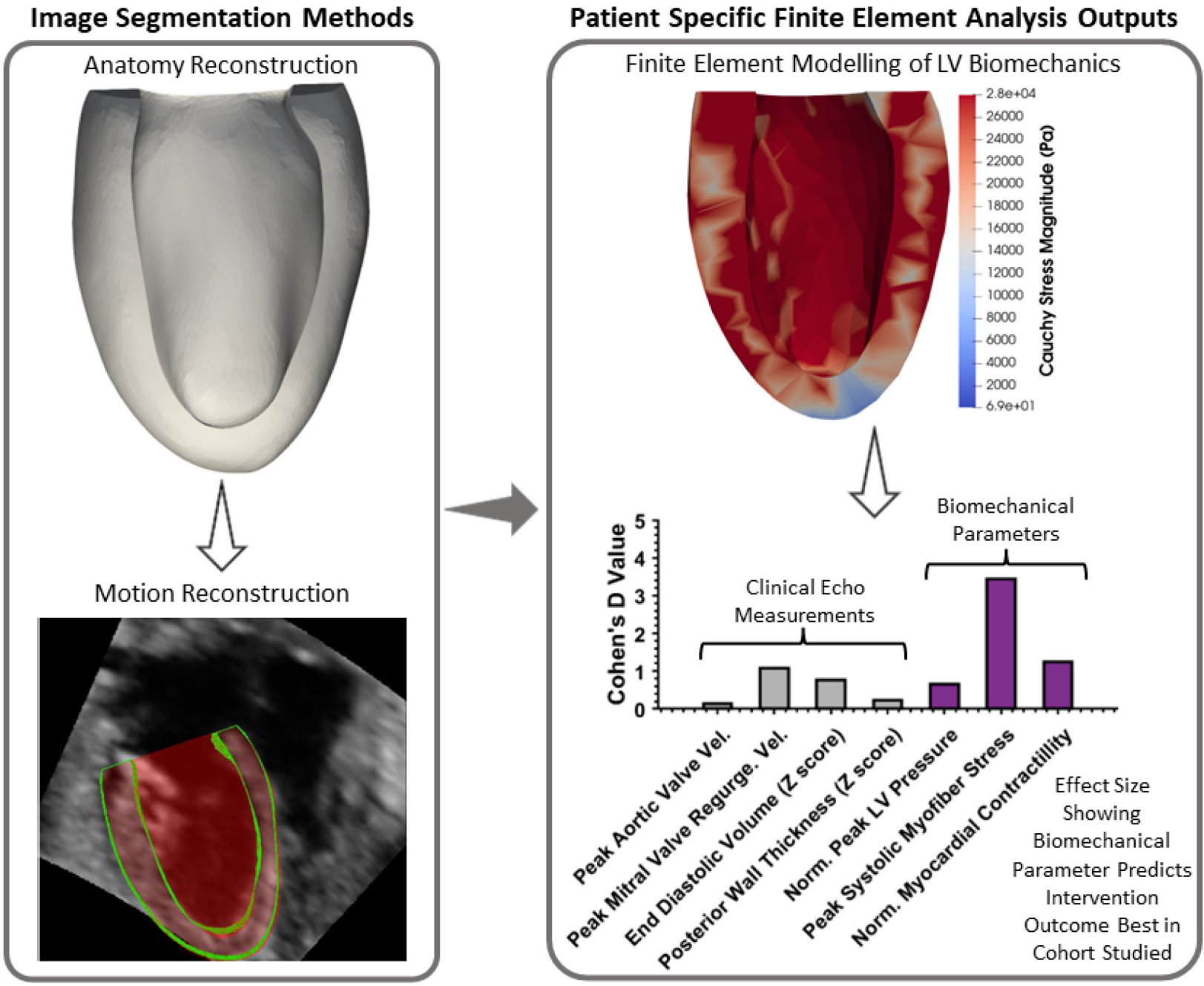

The Journal of Physiology

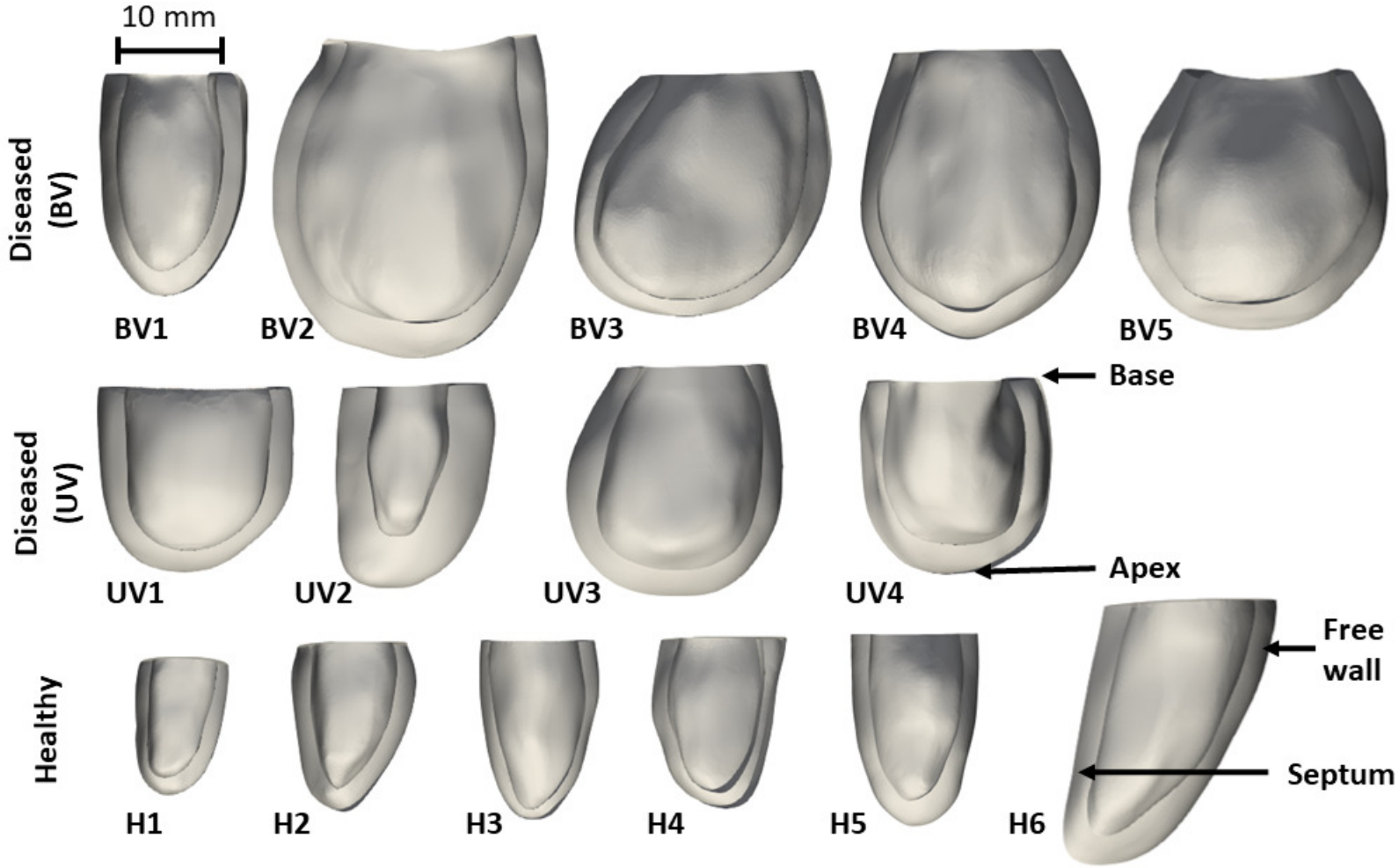
10 mm
Diseased (BV)
BV1
BV2
BV3
BV4
BV5
Diseased (UV)
Base
Apex
UV1
UV2
UV3
UV4
Healthy
Free wall
Septum
H1
H2
H3
H4
H5
H6

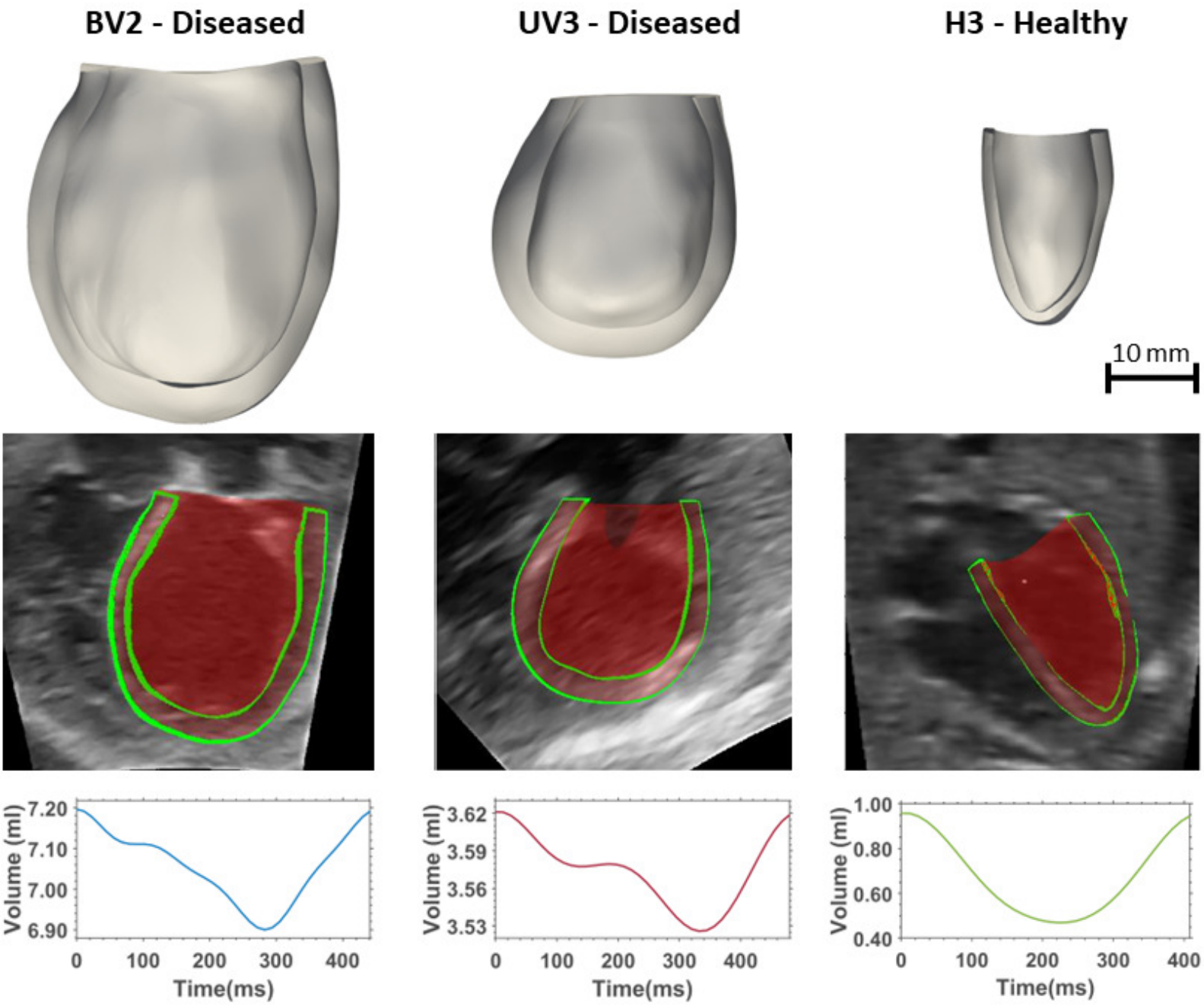
BV2 - Diseased
UV3 - Diseased
H3 - Healthy
10 mm
Volume (ml)
7.20
7.10
7.00
6.90
0
100
200
300
400
Time(ms)
Volume (ml)
3.62
3.59
3.56
3.53
0
100
200
300
400
Time(ms)
Volume (ml)
1.00
0.80
0.60
0.40
0
100
200
300
400
Time(ms)

A.

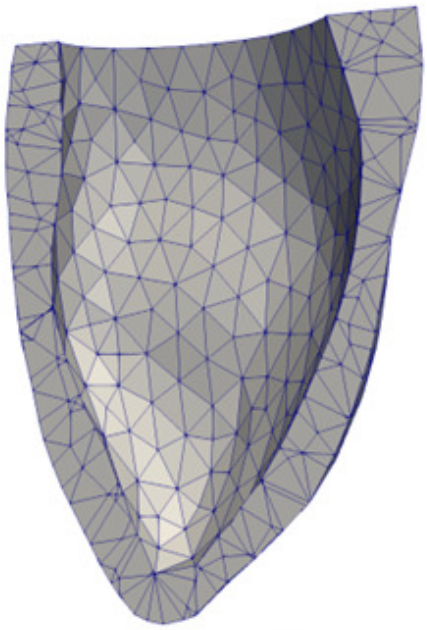

B.

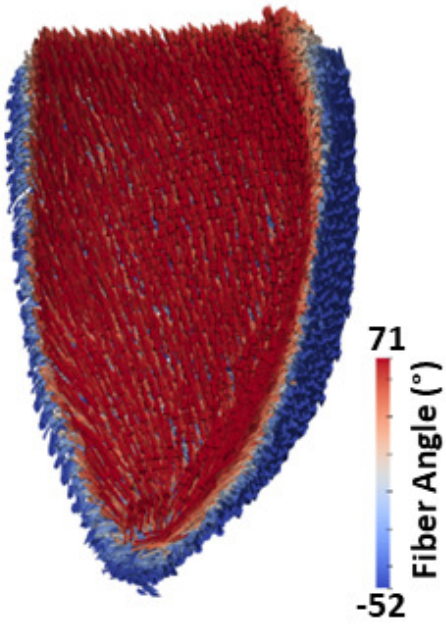
71
Fiber Angle (°)
-52

C.

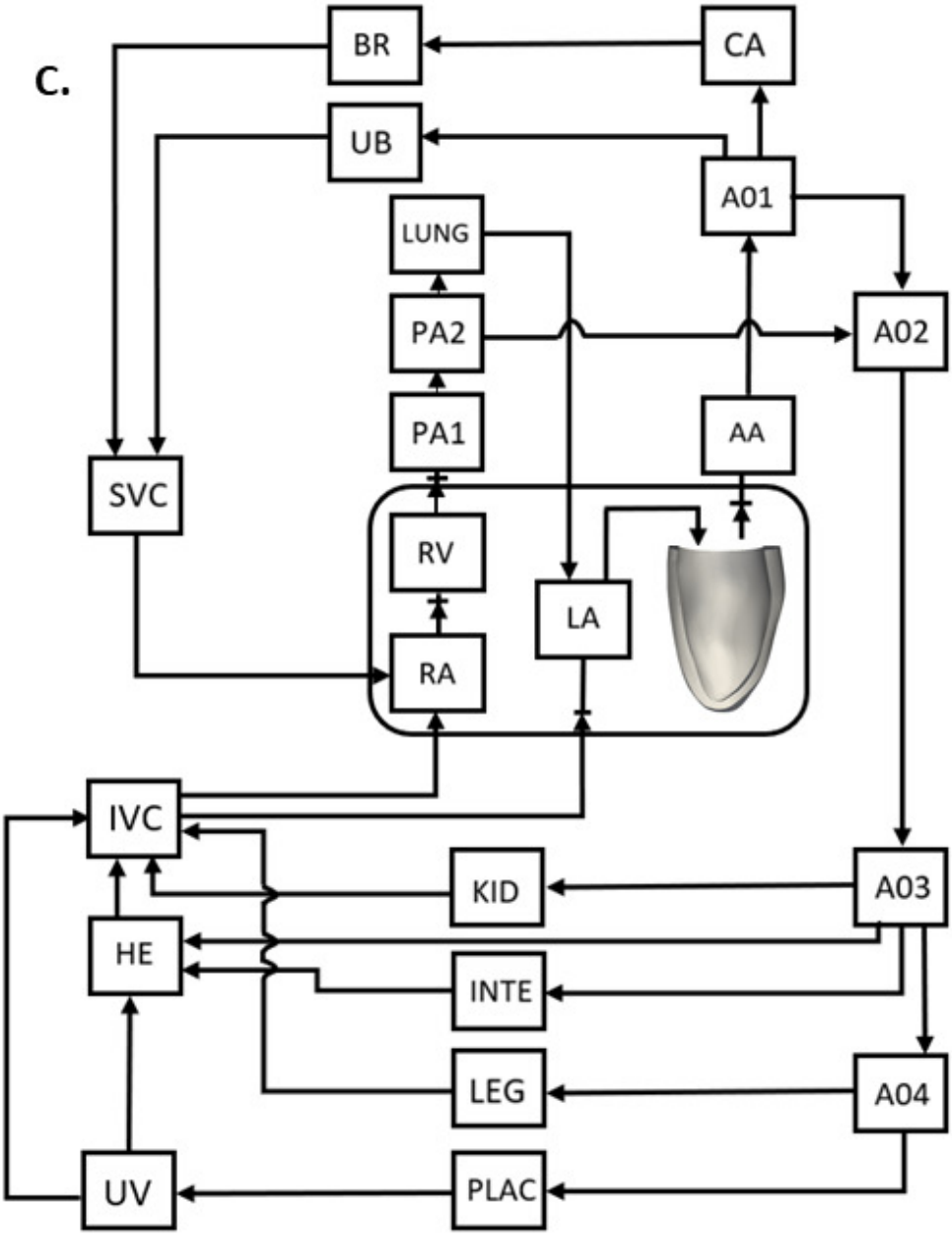
BR
CA
UB
A01
LUNG
PA2
A02
PA1
AA
SVC
RV
LA
RA
IVC
KID
A03
HE
INTE
LEG
A04
UV
PLAC

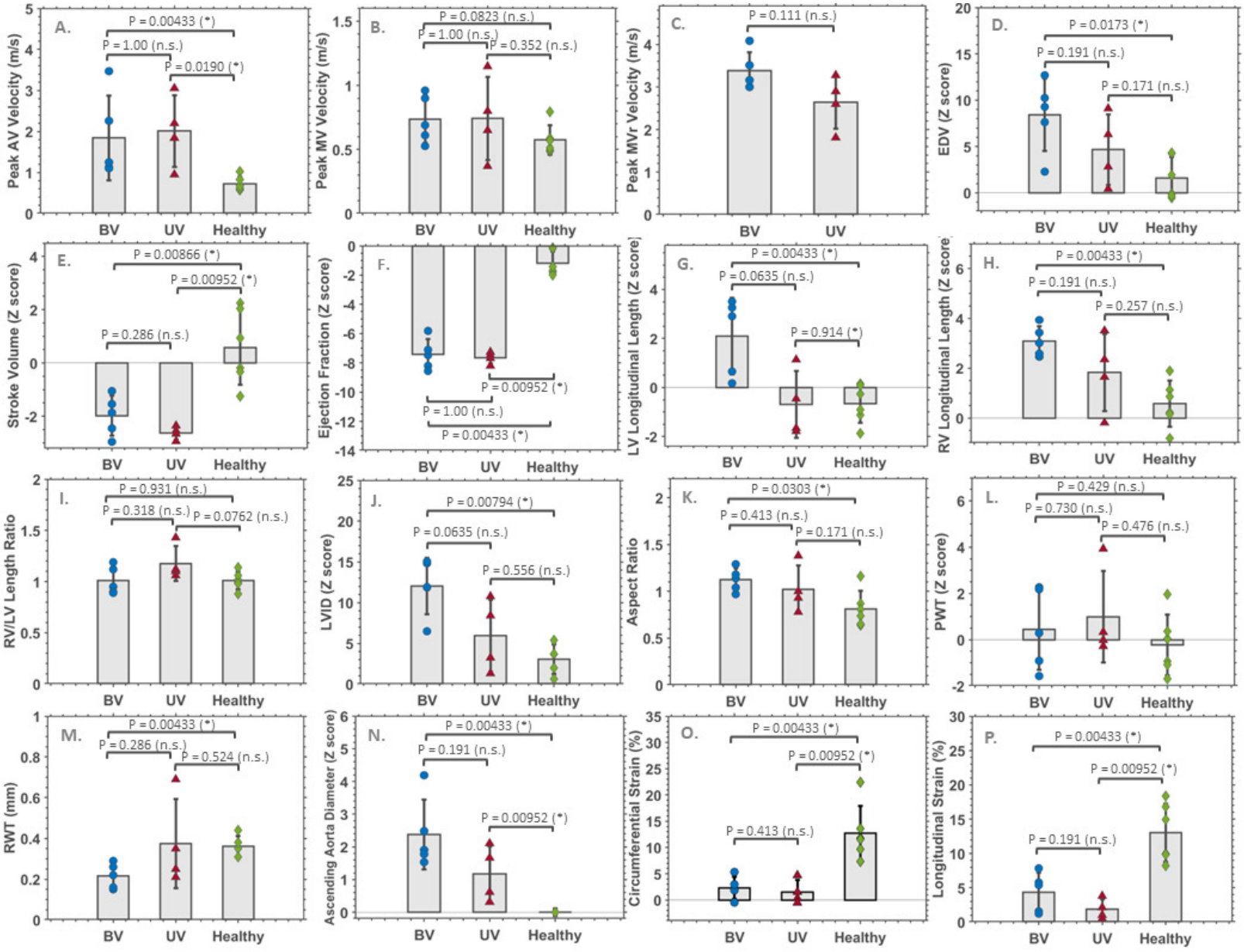
A.
Peak AV Velocity (m/s)
P = 0.00433 (*)
P = 1.00 (n.s.)
P = 0.0190 (*)
B.
Peak MV Velocity (m/s)
P = 0.0823 (n.s.)
P = 1.00 (n.s.)
P = 0.352 (n.s.)
C.
Peak MVr Velocity (m/s)
P = 0.111 (n.s.)
D.
EDV (Z score)
P = 0.0173 (*)
P = 0.191 (n.s.)
P = 0.171 (n.s.)
E.
Stroke Volume (Z score)
P = 0.00866 (*)
P = 0.00952 (*)
P = 0.286 (n.s.)
F.
Ejection Fraction (Z score)
P = 0.00952 (*)
P = 1.00 (n.s.)
P = 0.00433 (*)
G.
LV Longitudinal Length (Z score)
P = 0.00433 (*)
P = 0.0635 (n.s.)
P = 0.914 (*)
H.
RV Longitudinal Length (Z score)
P = 0.00433 (*)
P = 0.191 (n.s.)
P = 0.257 (n.s.)
I.
RV/LV Length Ratio
P = 0.931 (n.s.)
P = 0.318 (n.s.)
P = 0.0762 (n.s.)
J.
LVID (Z score)
P = 0.00794 (*)
P = 0.0635 (n.s.)
P = 0.556 (n.s.)
K.
Aspect Ratio
P = 0.0303 (*)
P = 0.413 (n.s.)
P = 0.171 (n.s.)
L.
PWT (Z score)
P = 0.429 (n.s.)
P = 0.730 (n.s.)
P = 0.476 (n.s.)
M.
RWT (mm)
P = 0.00433 (*)
P = 0.286 (n.s.)
P = 0.524 (n.s.)
N.
Ascending Aorta Diameter (Z score)
P = 0.00433 (*)
P = 0.191 (n.s.)
P = 0.00952 (*)
O.
Circumferential Strain (%)
P = 0.00433 (*)
P = 0.00952 (*)
P = 0.413 (n.s.)
P.
Longitudinal Strain (%)
P = 0.00433 (*)
P = 0.00952 (*)
P = 0.191 (n.s.)
BV
UV
Healthy

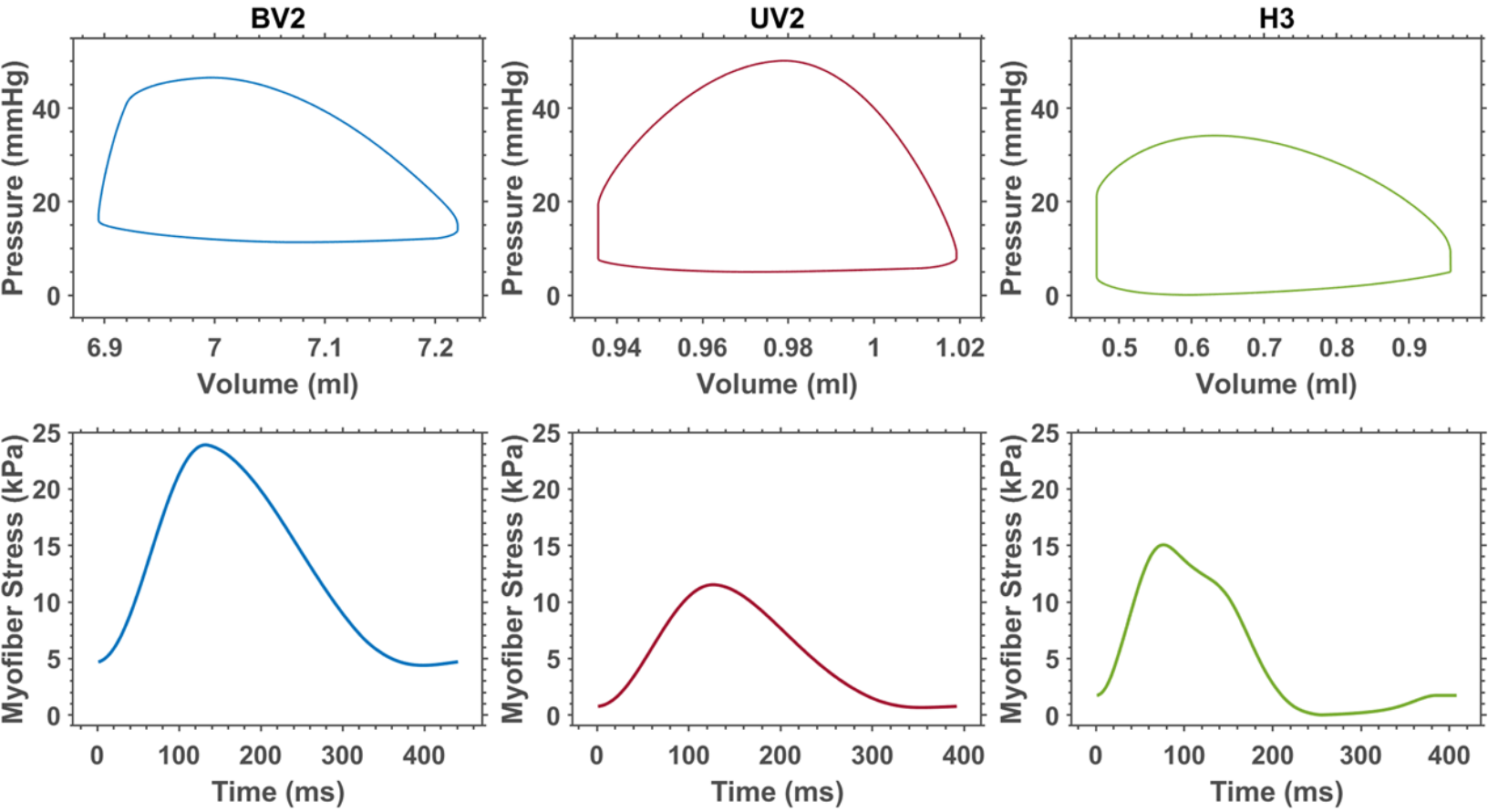
BV2
UV2
H3
Pressure (mmHg)
0
20
40
6.9
7
7.1
7.2
0.94
0.96
0.98
1
1.02
0.5
0.6
0.7
0.8
0.9
Volume (ml)
Myofiber Stress (kPa)
0
5
10
15
20
25
0
100
200
300
400
Time (ms)

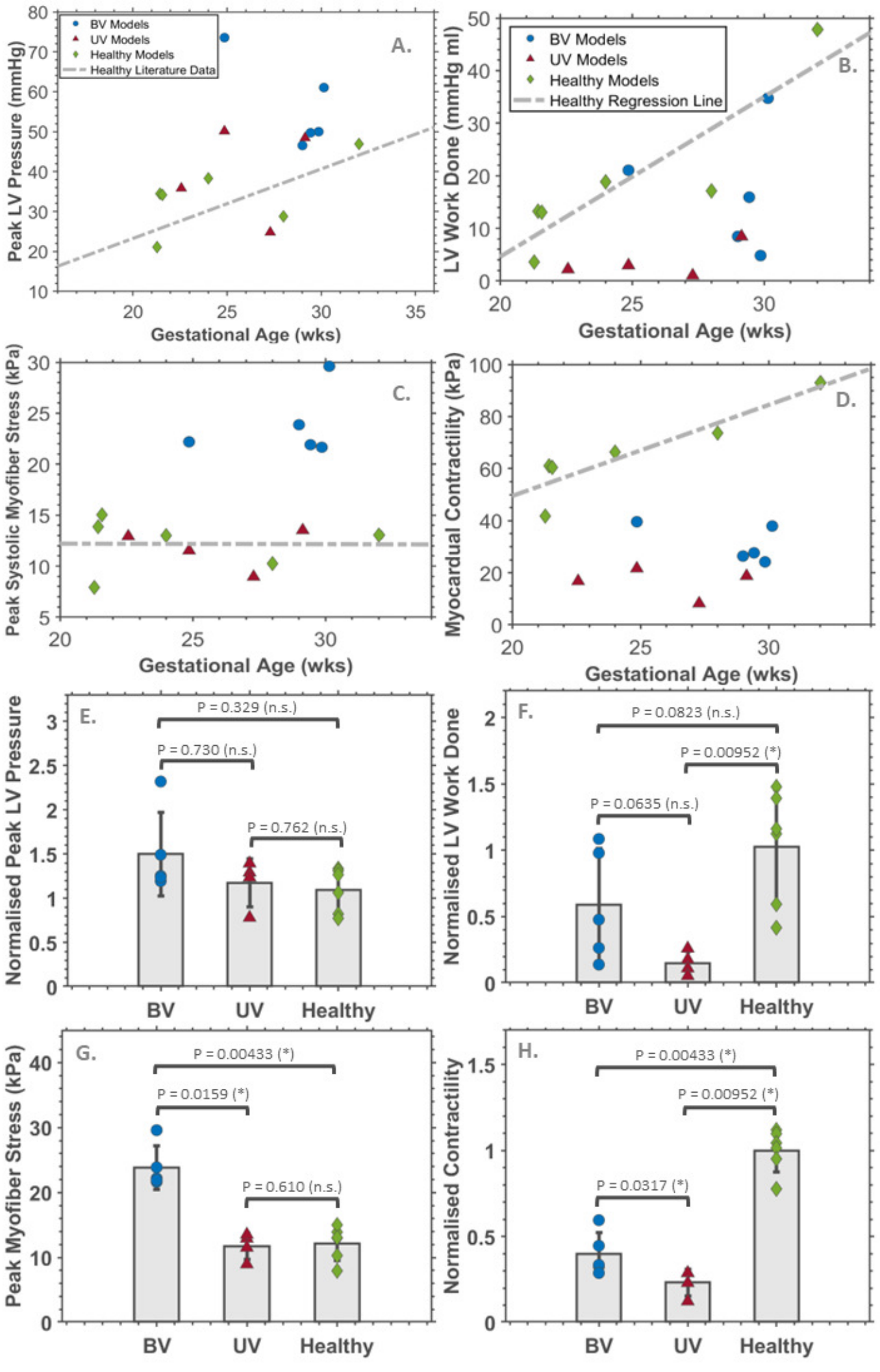
A.
BV Models
UV Models
Healthy Models
Healthy Literature Data
Peak LV Pressure (mmHg)
Gestational Age (wks)
B.
BV Models
UV Models
Healthy Models
Healthy Regression Line
LV Work Done (mmHg ml)
Gestational Age (wks)
C.
Peak Systolic Myofiber Stress (kPa)
Gestational Age (wks)
D.
Myocardual Contractility (kPa)
Gestational Age (wks)
E.
P = 0.329 (n.s.)
P = 0.730 (n.s.)
P = 0.762 (n.s.)
Normalised Peak LV Pressure
BV
UV
Healthy
F.
P = 0.0823 (n.s.)
P = 0.00952 (*)
P = 0.0635 (n.s.)
Normalised LV Work Done
BV
UV
Healthy
G.
P = 0.00433 (*)
P = 0.0159 (*)
P = 0.610 (n.s.)
Peak Myofiber Stress (kPa)
BV
UV
Healthy
H.
P = 0.00433 (*)
P = 0.00952 (*)
P = 0.0317 (*)
Normalised Contractility
BV
UV
Healthy

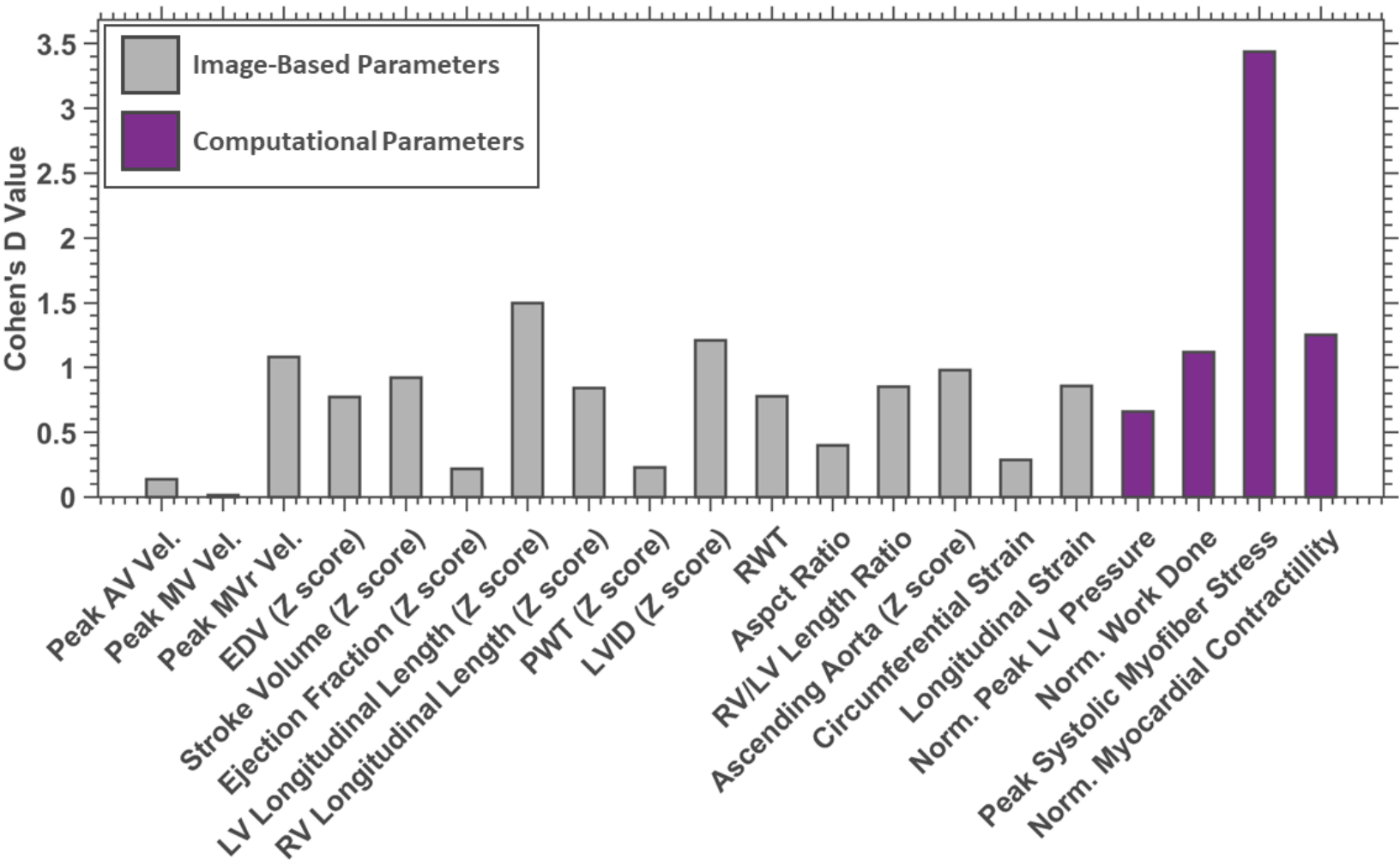
Image-Based Parameters
Computational Parameters
Cohen's D Value
3.5
3
2.5
2
1.5
1
0.5
0
Peak AV Vel.
Peak MV Vel.
Peak MVr Vel.
EDV (Z score)
Stroke Volume (Z score)
Ejection Fraction (Z score)
LV Longitudinal Length (Z score)
RV Longitudinal Length (Z score)
PWT (Z score)
LVID (Z score)
RWT
Aspct Ratio
RV/LV Length Ratio
Ascending Aorta (Z score)
Circumferential Strain
Longitudinal Strain
Norm. Peak LV Pressure
Norm. Work Done
Peak Systolic Myofiber Stress
Norm. Myocardial Contractility

A.

Image Based Characteristic Correlated with Peak Systolic Myofiber Stress	r Value
Peak AV Velocity	-0.15
Peak MVr Velocity	0.66
LV Longitudinal Length	0.67
RV Longitudinal Length	0.81
LVID	0.63
RWT	-0.50
EDV	0.67
SV	0.81

B.

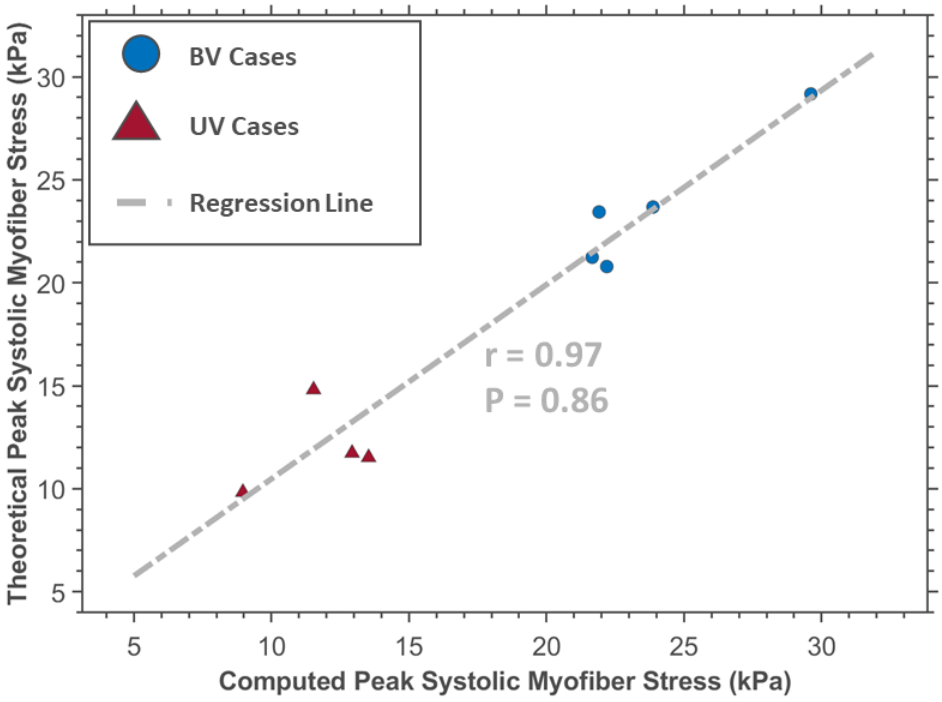

Marker	Parameter	AUC	P Value (Parameter-Estimated Peak Systolic Myofiber Stress)
	Estimated Peak Systolic Myofiber Stress	0.91	-
	LV Longitudinal Length Z Score	0.84	0.4322 (n.s.)
	EDV Z Score	0.83	0.4115 (n.s.)
	Stroke Volume Z Score	0.82	0.3304 (n.s.)
	RV Longitudinal Length Z Score	0.77	0.1579 (n.s.)
	LVID Z Score	0.76	0.1432 (n.s.)
	RV/LV Length Ratio	0.73	0.1015 (n.s.)
	RWT	0.69	0.0494 (*)
	MVr Velocity	0.63	0.0171 (*)
	Estimated Pressure	0.53	0.0016 (*)
	AV Velocity	0.53	0.0011 (*)